Available online at www.sciencedirect.com
ScienceDirect
Trans. Nonferrous Met. Soc. China 30(2020) 1315−1324
Transactions of Nonferrous Metals Society of China
www.tnmsc.cn

Improvement of microstructure and mechanical properties of TiAl−Nb alloy by adding Fe element

Yong YANG[1,2], He-ping FENG[3], Qi WANG[1], Rui-run CHEN[1], Jing-jie GUO[1], Hong-sheng DING[1], Yan-qing SU[1]

1. School of Materials Science and Engineering, Harbin Institute of Technology, Harbin 150001, China;
2. Department of Materials Engineering, Baotou Vocational & Technical College, Baotou 014030, China;
3. The fifth Branch Company, Inner Mongolia First Machinery Group Corporation Limited, Baotou 014032, China

Received 12 October 2019; accepted 14 April 2020

Abstract: In order to improve mechanical properties and optimize composition of TiAl−Nb alloys, Ti46Al5Nb0.1B alloys with different contents of Fe (0, 0.3, 0.5, 0.7, 0.9, and 1.1 at.%) were prepared by melting. Macro/microstructure and compression properties of the alloys were systematically investigated. Results show that Fe element can decrease the grain size, aggravate the Al-segregation and also form the Fe-rich *B*2 phase in the interdendritic area. Compressive testing results indicate that the Ti46Al5Nb0.1B0.3Fe alloy shows the highest ultimate compressive strength and fracture strain, which are 1869.5 MPa and 33.53%, respectively. The improved ultimate compression strength is ascribed to the grain refinement and solid solution strengthening of Fe, and the improved fracture strain is due to the reduced lattice tetragonality of γ phase and grain refinement of the alloys. However, excessive Fe addition decreases compressive strength and fracture strain, which is caused by the severe Al-segregation.

Key words: TiAl alloy; Fe; *B*2 phase; microstructure; mechanical properties

1 Introduction

TiAl−Nb alloys are considered to have great possibility to take the place of nickel-based blades in turbine engines, mainly due to their low density and excellent high-temperature mechanical properties [1−4]. Even so, their poor ductility and crack resistance below 800 °C still hinder the applications of these materials [5−7]. With respect to obtaining balanced mechanical properties for strength and ductility, several methods have been used, including heat treatment, thermo-mechanical treatments, addition of alloying elements, and forming composites in TiAl−Nb alloys [8−10]. In these methods, addition of substitutional or interstitial atoms into TiAl−Nb alloys has received great attention in recent two decades [11−14].

Among the alloying elements, Fe is well known to be a strong β-stabilizing element, and its β-stabilizing effect is even higher than that of Nb, Ta, Cr and Mo. The addition of Fe to TiAl alloys can enhance the liquidity and then improve their castability [15,16]. A small amount of Fe addition (not more than 0.5 at.%) to binary TiAl alloys can improve the tensile strength, ductility and creep resistance effectively [11]. The solid solution strengthening of Fe in TiAl alloys results in the improved strength and ductility because Fe can increase the Ti 3s and Al 2s binding energies of the γ phase. However, Fe decreases the Ti 3p and Al 2p binding energies in the Ti−Ti, Ti−Al and Al−Al bonds of the γ phase, thus improving the creep resistance. QIU et al [16,17] have demonstrated that

Foundation item: Project (2017YFA0403802) supported by the National Key Research and Development Program of China; Project (51825401) supported by the National Natural Science Foundation of China; Project (2019TQ0076) supported by the China Postdoctoral Science Foundation

Corresponding author: Rui-run CHEN; Tel/Fax: +86-451-86413931; E-mail: ruirunchen@hit.edu.cn

DOI: 10.1016/S1003-6326(20)65298-0

the addition of Fe refines the grain and results in high ductility of TiAl alloys at 790 °C. The stabilized *B*2 phase by Fe retards the growth of α phase, and then leads to grain refinement. During the deformation, the high-temperature β phase can facilitate grain boundary sliding and grain rotation because it becomes soft at elevated temperatures, therefore resulting in the TiAl alloys exhibiting high ductility at 790 °C. Addition of too much Fe (5 at.%) can transform the brittle α_2 (Ti_3Al) phase of the TiAl alloys into intermetallic τ_2 (Al_2FeTi) phase, which can improve the room-temperature strength and the hot workability of the TiAl alloys [18,19]. Additionally, the microstructure of the TiAl−Nb alloys can effectively be refined by the B element. However, few studies have been conducted on the influence of Fe on the mechanical properties of the TiAl−Nb alloys.

For the improvement of the mechanical properties and the optimization of the composition of TiAl−Nb alloys, the Ti46Al5Nb0.1B alloy, which has lower *B*2 phase and different solidification paths compared to the TiAl−Nb alloy with low Al content, was chosen as the base alloy to investigate the effect of Fe on the phase constitution, macro/microstructure and mechanical properties of TiAl−Nb alloys. Particular attention is paid to the strengthening mechanism of Fe element on TiAl−Nb alloys.

2 Experimental

The Ti46Al5Nb0.1B*x*Fe button ingots (~60 g) were prepared by non-consumable arc-melting under high-purity argon atmosphere. The values of *x* are 0, 0.3, 0.5, 0.7, 0.9 and 1.1 at.%. Therefore, these alloys will be referred to as 0Fe, 0.3Fe, 0.5Fe, 0.7Fe, 0.9Fe and 1.1Fe alloys, respectively. The raw materials are titanium sponge, pure aluminum, iron powder, boron powder and Al−Nb alloy (72.65 wt.% Nb). The raw materials were mixed and pressed into round cakes with a diameter of 30 mm at room temperature, which can effectively reduce the loss of the raw materials during the melting. To promote chemical composition homogeneity and to avoid the influence of cooling rate on microstructures, we used the same melting process to melt all the ingots five times during the melting. The ingots were cut vertically from the center area by an electro-discharge machine. The specimens were polished and etched by solution consisting of HF, HNO_3 and H_2O with a volume ratio of 5:15:80.

The macrostructures of the alloys were investigated by Nikon D800 digital camera. The line-intercept method was used to obtain the average width of columnar grains in the middle region of the ingots. The specimens for microstructural observation and mechanical testing were taken from similar positions in the ingots. The phase constitutions of the alloys were analyzed by X-ray diffraction (XRD) with Cu K_α radiation (λ=0.154056 nm), the scanning speed was 4 (°)/min, and the 2θ range was 20°−90°. The lattice parameters and the relative volume fractions of the different phases were calculated by the Java Agent Development Framework (JADE) from the results of XRD [20]. The microstructures were investigated by optical microscope (OM) and scanning electron microscope (SEM, Quanta 200F), and the phase compositions were identified by energy dispersive spectrometer (EDS).

Room-temperature compression tests were operated on an 5569 Instron machine with a constant strain rate of 0.5 mm/min. The compressive testing specimens were *d*5 mm × 7.5 mm cylinders, and each test was conducted three times to obtain the mean value. In order to get accurate compressive strength and fracture strain, the surfaces of the samples were ground parallel to the other before testing.

3 Results

3.1 Macrostructure of Ti46Al5Nb0.1B alloy with different Fe contents

Figure 1 shows the macrostructures taken from the longitudinal sections of the center area of the button ingots with different Fe contents. It can be found that the macrostructure of the alloys is mainly composed of columnar grains. In order to examine the refinement effect of the Fe element on Ti46Al5Nb0.1B alloys, the average widths of columnar grains were measured, as presented in Fig. 2. The average width of columnar grains of the Fe-containing TiAl alloys is smaller than that of the Fe-free alloy, and it decreases with increasing Fe content. It is known that the cubic β is the primary solidification phase in the TiAl alloys when the content of Al is less than 49.3 at.%. During the

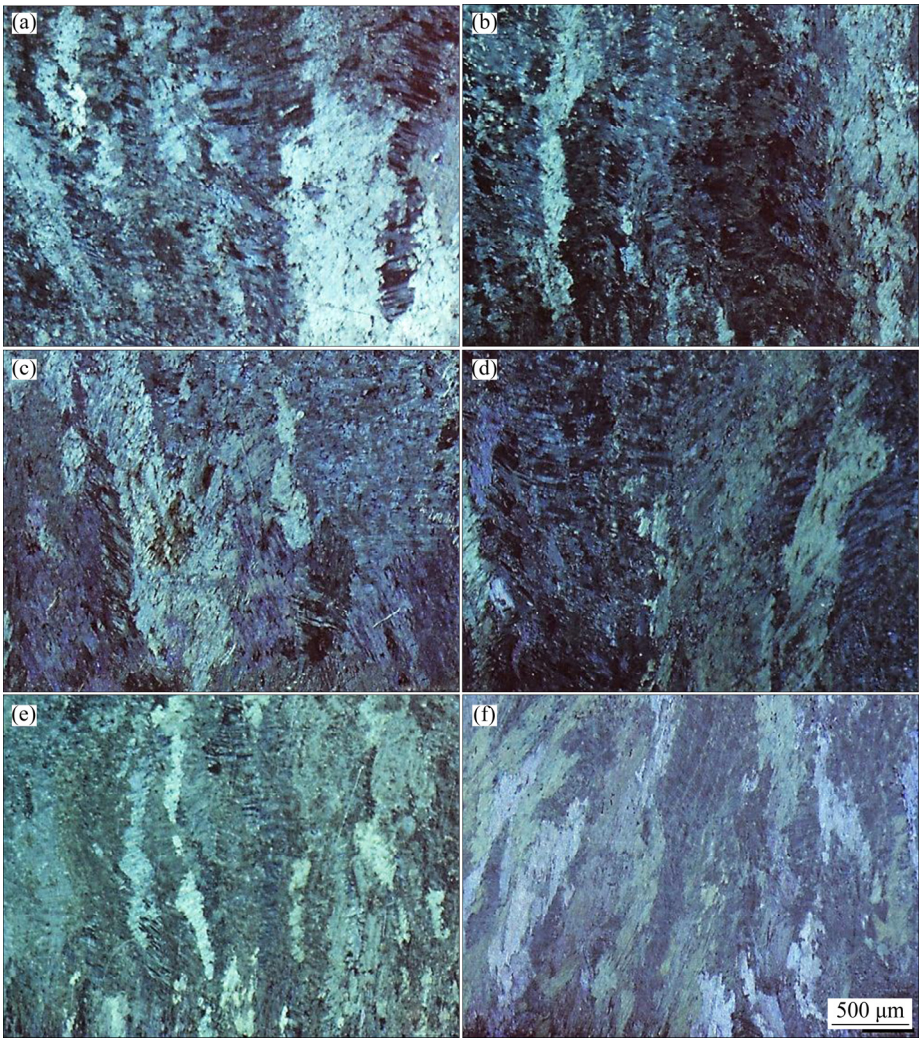

Fig. 1 Macrostructures taken from longitudinal section in center area of ingots with different Fe contents: (a) 0 at./% Fe; (b) 0.3 at.% Fe; (c) 0.5 at.% Fe; (d) 0.7 at.% Fe; (e) 0.9 at.% Fe; (f) 1.1 at.% Fe

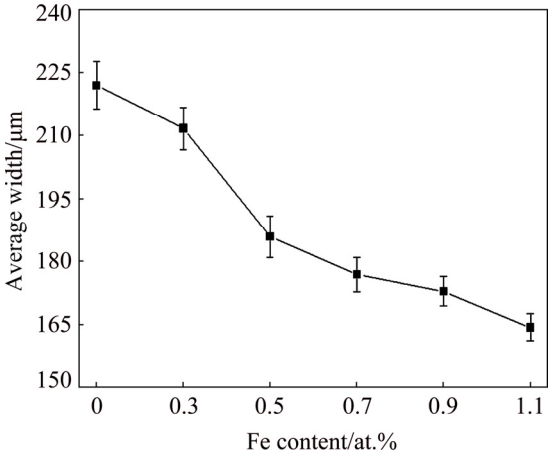

Fig. 2 Variation of average width of columnar grain with Fe content

solidification, the stabilizers such as Fe and Nb segregated in the primary β phase, but Al was rejected from the β phase into the liquid and formed an Al-rich layer ahead of the solidification front. The Al content ahead of the solid front increased with the increase of Fe content and then led to the increase in constitutional supercooling. The increased supercooling promoted the formation of primary β phase, thus the microstructures of the Fe-containing TiAl alloys were refined. Recently, similar results for the ternary Ti−Al−Fe alloy system have been reported by several other researchers [16,21].

3.2 Microstructure of Ti46Al5Nb0.1B alloy with different Fe contents

Figure 3 shows the XRD patterns of the alloys. The α_2 and γ can be identified for the alloys. Bragg peaks of $B2$ phase can also be observed for the alloys except for the Fe-free and 0.3Fe alloys. Maybe the relatively low volume fraction of $B2$

phase cannot be detected by X-ray diffraction. However, the τ_2 phase is not found, which is not consistent with the results in Refs. [18,19], which reported that the Fe-rich τ_2 phase was formed with the addition of Fe. The possible reason is that addition minor of Fe to the base alloy is not enough to transform the α_2 phase to τ_2 phase.

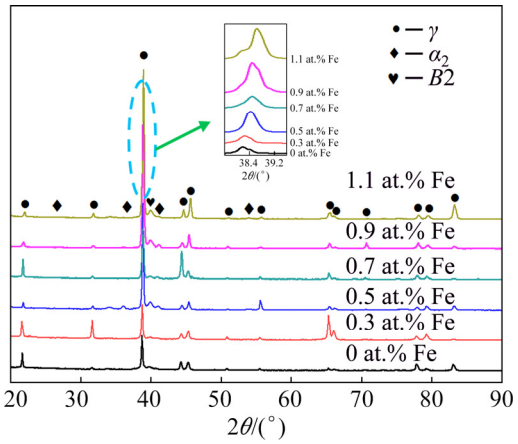

Fig. 3 XRD patterns of alloys with different Fe contents

Table 1 shows the variation of α_2, γ and $B2$ volume fractions with different Fe contents. The volume fraction of $B2$ phase increases with the increase of Fe content, and it increases from 0.9% to 2.9% when the Fe content increases from 0 to 1.1 at.%. This increasing tendency can also be verified by SEM microstructures. With the increase of Fe content, the volume fraction of the γ phase increases while the volume fraction of α_2 decreases. These results are consistent with previous studies, which reported that the addition of some heavy metal elements to TiAl alloys could increase the amount of the γ phase [16,22,23].

It can be seen in the inset of Fig. 3 that the peak position of the TiAl (111) plane shifts to higher 2θ value with the increase of Fe content,

Table 1 Volume fractions of α_2, γ and $B2$ phase with different Fe contents

Content of Fe/at.%	Volume fraction/%		
	α_2	$B2$	γ
0	28.5	0.9	70.6
0.3	26.8	1.3	71.9
0.5	23.9	1.8	74.2
0.7	22.6	2.2	75.2
0.9	21.1	2.5	76.4
1.1	18.5	2.9	78.7

which implies the change of lattice parameters. Figure 4 shows the lattice parameters and tetragonality of the γ phase in Ti46Al5Nb0.1BxFe alloys with different Fe contents. The lattice parameters of a-axis increase but those of the c-axis decrease with the increase of Fe content. The shrunk c-axis and the expanded a-axis indicate the decrease of the c/a ratio of the crystal lattice, and therefore the reduced lattice tetragonality of TiAl, as shown in Fig. 4. The experimental results and first principle calculations on the occupation site of alloy elements reveal that Fe exclusively occupies the Al sites in the γ phase [24,25]. It is easy to understand that the lattice parameters of the γ phase unit cell change because Fe has smaller atomic radius (127 pm) than Al (143 pm) does.

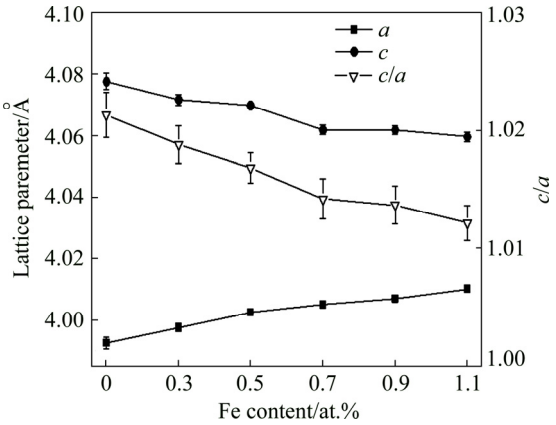

Fig. 4 Lattice parameters and tetragonality of γ phase in alloys with different Fe contents

Figure 5 shows the typical SEM−BSE micrographs of the Ti46Al5Nb0.1BxFe alloys. A wide variety of microstructures can be observed from the BSE images of the as-cast ingots. The microstructure of the Fe-free alloy is composed of a grey matrix and black regions, as shown in Fig. 5(a). The grey region exhibiting full lamellar microstructures is the primary dendrite morphology. The interdendritic areas or the triple junctions of the primary solidified β dendrites are composed of the black regions, which are enriched in Al. When increasing the Fe content to 0.3 at.%, the white particles are occasionally found at the boundary of the grey matrix, as shown in Fig. 5(b). With further increasing the Fe content, the white particles in the interdendritic areas are remarkably increased, as shown in Figs. 5(c−f).

The EDS results (Fig. 6) combined with the XRD results indicate that the white particles are

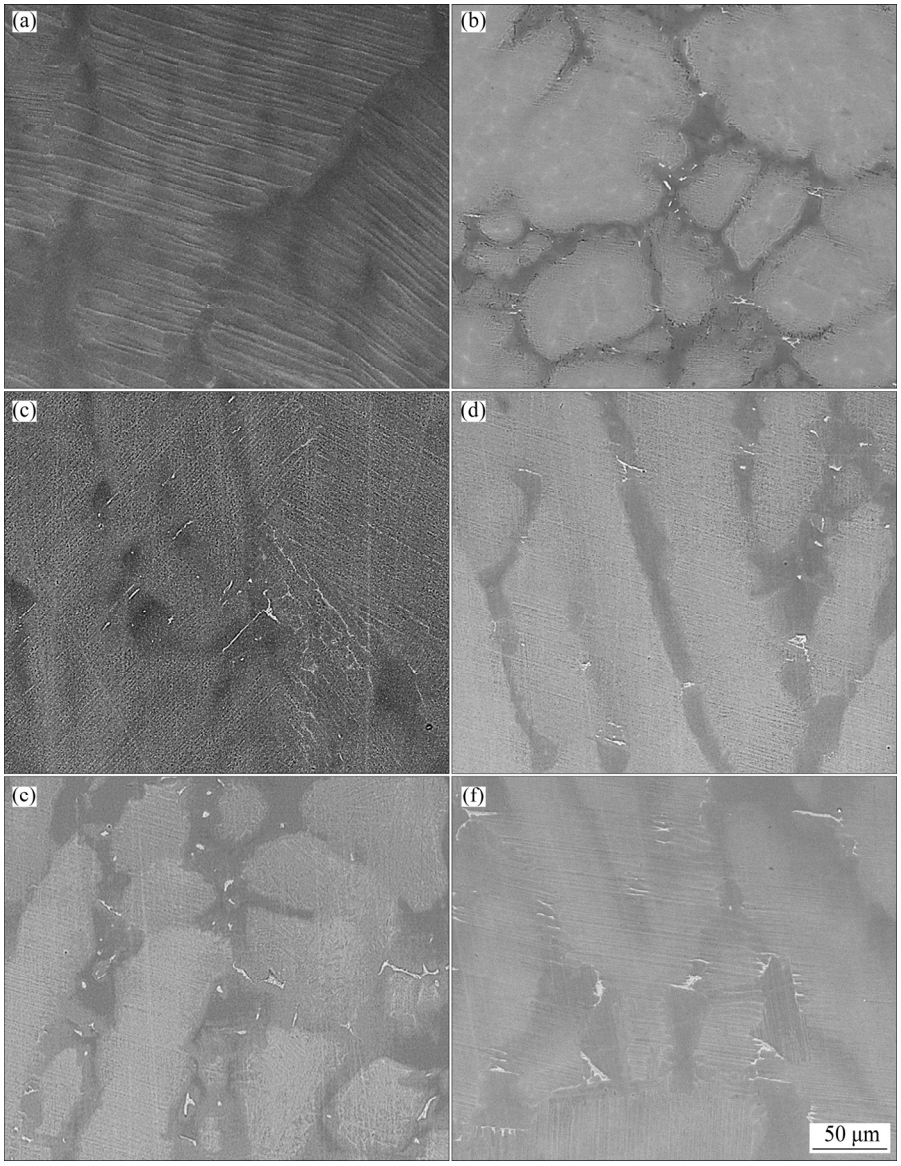

Fig. 5 SEM−BSE images of alloys with different Fe contents: (a) 0 at.% Fe; (b) 0.3 at.% Fe; (c) 0.5 at.% Fe; (d) 0.7 at.% Fe; (e) 0.9 at.% Fe; (f) 1.1 at.% Fe

enriched in Fe, which are the Fe-rich *B*2 phase, and they are also found in the ternary Ti−Al−Fe alloys [16,21]. It can be inferred from the EDS results that the Fe content in the *B*2 phase increases with the increase of Fe addition. As the Fe content further increases, the Fe-rich *B*2 phase in the interdendritic areas increases, and the shape of it changes from band-like to block shape, as shown in Fig. 5.

3.3 Compression properties and fractography

In order to evaluate the alloying effect of Fe, the compressive strength and fracture strain for all the alloys at room temperature were obtained from constant strain rate compression tests. The relationship between ultimate compressive strength (σ_{UCS}) and fracture strain (ε_f) with different Fe contents is shown in Fig. 7. When increasing the Fe content to 0.3 at.%, both the σ_{UCS} and ε_f increase, but they gradually decrease with further increase of Fe content. The 0.3Fe and 0.5Fe alloys have higher σ_{UCS} and ε_f compared with the Fe-free alloy and the alloys with higher Fe additions. The maximum σ_{UCS} and ε_f are achieved by addition of 0.3 at.% Fe, which are 1869.5 MPa and 33.53%, respectively. They are 150 MPa and 4.1% higher than those of the Fe-free alloy, respectively. The 0.7Fe alloy exhibits σ_{UCS} and ε_f comparable to the Fe-free alloy. When further increasing the Fe content (>0.7 at.%), the σ_{UCS} and ε_f decrease rapidly.

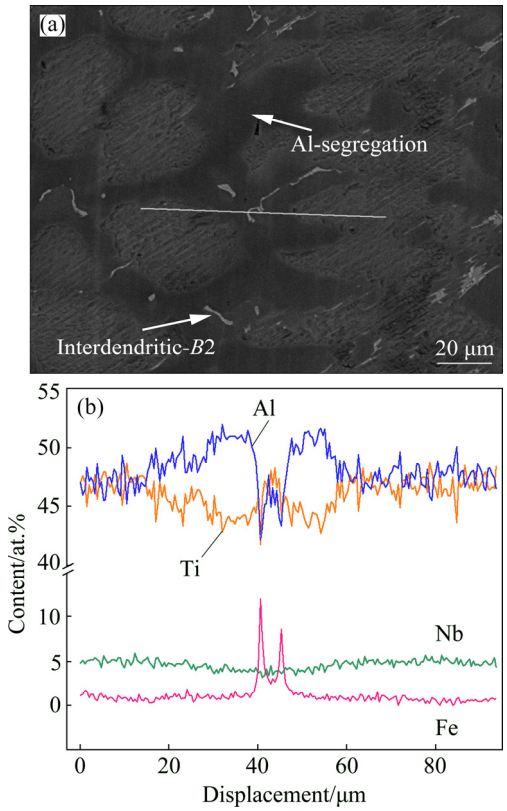

Fig. 6 Line scanning across dendrites in Ti46Al5Nb-1.1Fe0.1B alloy (a), and element distributions along white line in (a) (b)

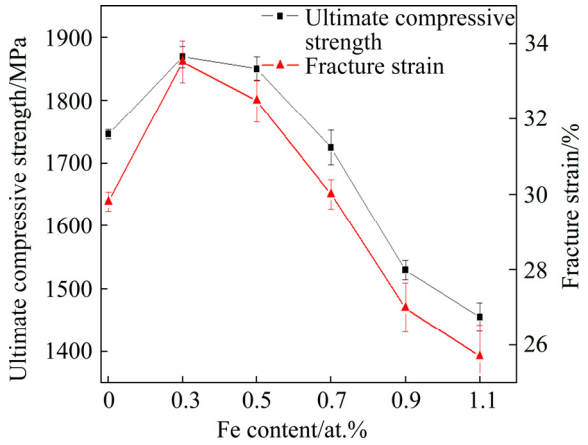

Fig. 7 Variation of ultimate compressive strength and fracture strain of alloys with Fe content

When the Fe content is in the range of (0.5−0.7) at.%, the σ_{UCS} and ε_f of the alloys gradually decrease, but are still higher than those of the Fe-free alloy. When further increasing Fe content to 1.1 at.%, the σ_{UCS} and ε_f of the alloy are even lower than those of the Fe-free alloy. One side of the failed compressed specimens was cut along the loading axis, then ground, polished, etched and examined to reveal the causes for the alloys with higher Fe content to exhibit lower mechanical properties. Figure 8(a) shows the side view of the 0.3Fe alloy specimen with the highest σ_{UCS} and ε_f. The crack propagates through the lamella and deflects when encountering obstacles, forming a tortuous crack path and rough fracture surfaces. This implies that the rough fracture surfaces are composed of a large amount of smooth shear cracking facets, which are located in different lamella layers with some steps connecting these facets. In the 0.5Fe alloy with the slightly lower σ_{UCS} and ε_f, the torn band-like γ phase is observed in the main crack, as marked by the white arrow in Figs. 8(b) and (c). In order to distinguish the torn band-like γ phase from the γ phase in the lamella colonies, we define this phase as γ'. Furthermore, in the 1.1Fe alloy which exhibits the lowest σ_{UCS} and ε_f, the equiaxed γ' grain with smooth surface is observed in the main shear crack (as shown in Fig. 8(d)). This indicates that the equiaxed γ' grain is torn by crack during compression.

4 Discussion

During the formation of primary β dendrites, because of the partition of solute K_β being less than 1, the β stablizers such as Fe and Nb will segregate into the β phase while Al is rejected into the interdendritic regions. As a result, the dendritic morphology of the primary β phase contains more Fe and Nb, and the interdendritic black areas are rich in Al. The EDS results clearly demonstrate the solidification microsegregation. Because of the high Al content in the interdendritic regions, the peritectic reaction $L+\beta\rightarrow\alpha$ occurs, producing the peritectic α phase enveloping the primary β phase, as shown in Table 2.

The schematic diagram is used to illustrate the peritectic reaction $L+\beta\rightarrow\alpha$ and the growth direction of the peritectic α phase, as shown in Fig. 9. When the primary β dendrites are covered with theperitectic α phase and isolated, the growth of the peritectic α phase occurs. α phase can be thickened by dissolving the primary β phase as well as the precipitation towards the interdendritic liquid. If the Al content in the liquid is high enough, the α phase will precipitate from the liquid directly. Upon cooling, although most of Fe and Nb are concentrated in the β dendrites, the rest of them stay

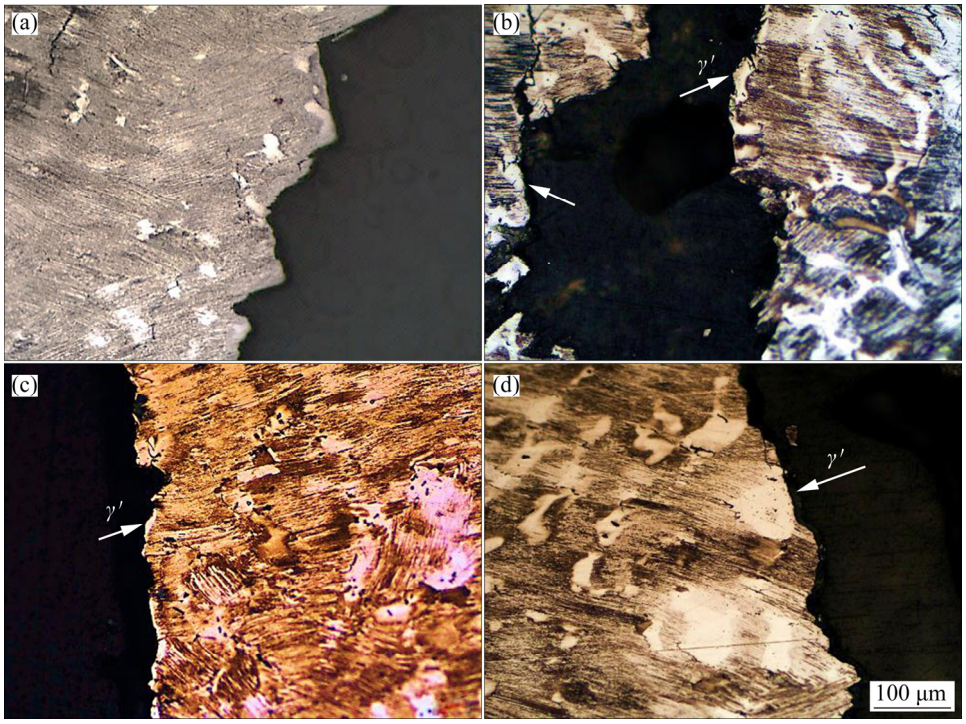

Fig. 8 Optical micrographs of side-view of fractured compressed specimens with different Fe contents: (a) 0.3 at.% Fe; (b) 0.5 at.% Fe; (c) 0.7 at.% Fe; (d) 1.1 at.% Fe

Table 2 Average compositions in different zones of Ti46Al5Nb1.1Fe0.1B alloy by EDS

Location	Content/at.%			
	Ti	Al	Nb	Fe
Dendritic arm	47.43	46.35	5.13	1.09
Interdendritic arm	43.46	51.05	4.51	0.97
Fe-rich region	44.32	43.38	3.70	8.59

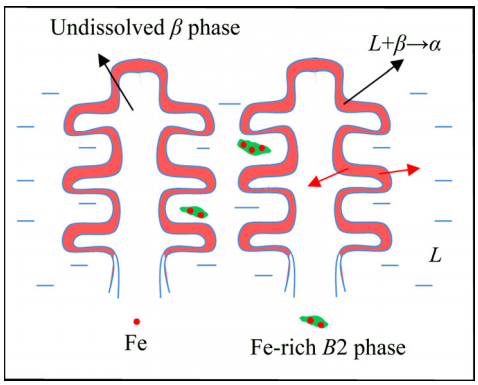

Fig. 9 Schematic diagram of peritectic reaction and growth direction of peritectic α phase

in the interdendritic regions. As the Al atoms are diffused from liquid to α, the contents of the Fe and Nb elements in the interdendritic regions increase, and they are easily saturated and diffused with more difficulty due to the faster cooling rate caused by the water-cooled copper crucible. As the temperature further decreases, the diffusion of Fe and Nb in the interdendritic region becomes more difficult. Therefore, they tend to participate in the form of Fe-rich $B2$ particles from the last liquid in the interdendritic regions [26], as shown in Fig. 9.

The increase of Fe addition leads to the higher Fe content in the interdendritic region. Therefore, the volume fraction of the Fe-rich $B2$ phase increases. With the continuous cooling, the primary β phase transforms into full lamellar structure of α_2/γ by the $\beta\rightarrow\alpha\rightarrow\alpha_2/\gamma$ solid-state phase transformation. The residual interdendritic liquid with higher Al content will form a large amount of γ grains (γ') after cooling to room temperature [26−28], as shown in Fig. 5. The EDS results also indicate that the solution of Fe in the $\alpha_2+\gamma$ matrix increases with increasing Fe content. It can be concluded that the solidification path of the Ti46Al5Nb0.1BxFe alloys is $L\rightarrow L+\beta\rightarrow L+\beta+\alpha\rightarrow\beta+\alpha\rightarrow\alpha+B2\rightarrow\alpha_2+\gamma+B2$.

The reasons why the 0.3Fe alloy has the highest σ_{UCS} can be mainly ascribed to the following reasons. One main reason is the solid solution strengthening of Fe. EDS result shows that the Fe content with solid solute in the matrix increases with the increase of the Fe content, up to 1.1 at.% (Fig. 6). The atoms of Fe, Al and Ti have

different atomic radius. When the Fe occupies the Al sites in the unit cells of γ phase, a large misfit will be formed between the unit cells with Fe atoms and those without Fe atoms. It is obvious that the distortion in γ phase contributes to the solid solution strengthening and to the improvement of the strength. The other possible reason is the grain refinement by the Fe addition, and the fine-grain strengthening can be estimated by the Hall−Petch relationship.

It is well known that the ordered hexagonal structures of α_2 phase and the ordered faced-centered tetragonal structures of γ phase with few slip systems in them severely limit the motion of the dislocations, resulting in the low ductility of the TiAl alloys. Previous studies [29,30] have revealed that the lattice tetragonality of γ phase is closely related to the intrinsic brittleness of TiAl alloys. The reduced lattice tetragonality would result in fracture strain improvement because it could activate new operating glide systems in the γ phase. The XRD results show that the tetragonality (c/a) of γ phase is reduced with the addition of Fe, as shown in Fig. 4. Therefore, the other possible reason for the enhancement of the fracture strain with 0.3 at.% Fe addition is the reduction of the lattice tetragonality (c/a) of γ phase. Another possible reason for the improved fracture is related to the uniformity of the electron cloud distribution around Ti atoms in the lattice of the γ phase, because it can increase the severe limited dislocation glide of the γ phase under such a circumstance. Previous studies documented that, for the improvement of the ductility of TiAl alloys, the added alloying elements should substitute for the positions of the Al sublattice and have higher eletronegativities and smaller atomic radius than Ti and Al, respectively [31]. The atomic radii of the Ti, Al, Nb and Fe are 147, 143, 149 and 127 pm, respectively, and their eletronegativities are 1.50, 1.50, 1.60 and 1.83, respectively [32,33]. It is evident that Fe satisfies the above requirements, which then leads to the improvement of the uniformity of the electron cloud distribution around the Ti atoms in the lattice. Accordingly, the Ti46Al5Nb0.3Fe0.1B alloy exhibits higher strain than the Fe-free alloy. The refined columnar grains can also improve the fracture strain of the alloys. Therefore, the improved fracture strain of the 0.3Fe alloy results mainly from the reduced lattice tetragonality (c/a) of γ phase, the uniformity of electron cloud distribution of the γ phase, and refined grains.

It is clear from earlier work [34] that, during the compression process, the cracks can be retarded effectively by the tortuous crack path, hindering the premature fracture of the specimens. Therefore, the alloys with tortuous fracture surfaces exhibit the higher σ_{UCS} and ε_f. However, the soft γ phase in the TiAl alloy exhibits no tearing resistance and is detrimental for crack resistance because it inhibits the action of shear ligament toughening [34,35]. As the strain increases, the crack can easily propagate across the blocky γ phase and form a planar crack facet, as marked by the arrow in Fig. 8(d). The blocky γ phase on the crack propagation path can accelerate the growth rate of the crack propagation, resulting in the premature failure of the specimens during the compression test. The plastic deformation ability of the alloys decreases tremendously because of the premature fracture, and thus the σ_{UCS} and ε_f of the alloys decrease. For this reason, when the addition of Fe is higher than 0.3 at.%, the alloys exhibit lower compressive strength and fracture strain. The improved σ_{UCS} and ε_f of the alloys will be canceled out as Fe content is further increased, which is ascribed to the increased Al-segregation in the interdendritic region.

Previous studies [23,35,36] revealed that the Al-segregation cannot be eliminated completely by heat treatment in the single α phase region. Longer time and higher temperature are needed to increase the diffusion distance of the Al element, and then obtain the homogeneous microstructures. However, this method would not likely be beneficial to improving the mechanical properties of the as-cast alloys, because the fast growth rate of the α phase in the single α phase region leads to coarser lamellar colonies. The coarser grains will be harmful to the strength based on the Hall−Petch relationship. Therefore, the Al-segregation should be controlled in the interdendritic regions.

To achieve the optimum solid solution strengthening, the contents of the element's solid solute in the TiAl alloys should be as high as possible. However, the $B2$ phase in the TiAl alloys should be controlled because the $B2$ phase has been proved to be the cracking sources which deteriorate the room-temperature mechanical properties. SUN et al [11] proposed the [Cr] equivalent empirical equation, which can be used to evaluate the

capacity of elements to stabilize the *B*2 phase, and the formula is shown as follows:

$$[Cr]=aCr+bMn+(3/5)cV+(3/8)dNb+3/2(eW+f\,Mo)+3gFe \quad (1)$$

where *a*, *b*, *c*, *d*, *e*, *f* and *g* correspond to contents of alloying Cr, Mn, V, Nd, W, Mo and Fe elements, respectively.

Based on the above empirical equation, the optimum [Cr] equivalent content should be controlled within the range of (1.5−3.0) at.%. In our study, as the Fe content increases from 0.3 at.% to 0.5 at.%, the [Cr] is changed from 2.775 at.% to 3.375 at.%, and the strength and strain of the alloys show higher performance than others samples. This is consistent with the conclusion of SUN et al [11].

Therefore, the appropriate content range of Fe addition to the as-cast Ti46Al5Nb0.1B alloy is (0.3−0.5) at.%, at which the excellent mechanical properties can be achieved. This optimal composition range of Fe addition for the present high Nb-containing TiAl alloys is comparable to that of the binary TiAl alloys [11].

5 Conclusions

(1) The addition of Fe reduces the grain size of Ti46Al5Nb0.1B*x*Fe alloys: the width of columnar grains decreases from 223 to 164 μm by addition of 1.1 at.% Fe.

(2) The addition of Fe in Ti46Al5Al0.1B alloy results in the formation of Fe-rich *B*2 phase and aggravates Al-segregation in the interdendritic area. The volume fractions of both the *B*2 and *γ* phases increase with the increase of Fe content.

(3) When adding 0.3 at.% Fe to the Ti46Al5Al0.1B alloy, the alloy exhibits higher mechanical properties at room temperature: the ultimate compressive strength and fracture strain are 1869.5 MPa and 33.53%, respectively. Excessive Fe additions deteriorate strength and strain.

(4) The improved compression strength is attributed to the grain refinement strengthening and the solid solution strengthening of Fe, and the improved fracture strain is attributed to the reduced lattice tetragonality (*c*/*a*) of *γ* phase and refined grains. The decrease of the mechanical properties is attributed to the severe Al-segregation in the interdendritic area, which causes premature failure during the compression process.

References

[1] KOTHARI K, RADHAKRISHNAN R, WERELEY N M. Advances in gamma titanium aluminides and their manufacturing techniques [J]. Progress in Aerospace Sciences, 2012, 55: 1−16.

[2] LI Kai, CHEN Guang-yao, ZHANG Hao, ALI W, LU Xiong-gang, LI Chong-he. Microstructure evolution of directionally solidified Ti−46Al−8Nb alloy in the $BaZrO_3$-based mould [J]. Materials Research Express, 2018, 5(11): 1−12.

[3] ISMAEEL A, WANG C S. Effect of Nb additions on microstructure and properties of *γ*-TiAl based alloys fabricated by selective laser melting [J]. Transactions of Nonferrous Metals Society of China, 2019, 29: 1007−1016.

[4] FANG Hong-ze, CHEN Rui-run, YANG Yong, SU Yan-qing, DING Hong-sheng, GUO Jing-jie, FU Heng-zhi. Role of graphite on microstructural evolution and mechanical properties of ternary TiAl alloy prepared by arc melting method [J]. Materials & Design, 2018, 156: 300−310.

[5] ZHANG S Z, SONG Z W, HAN J C, ZHANG C J, LIN P, ZHU D D, KONG F T, CHEN Y Y. Effect of 2−6 at.% Mo addition on microstructural evolution of Ti−44Al alloy [J]. Journal of Materials Science & Technology, 2018, 34(7): 138−146.

[6] LIU Z C, LIN J P, LI S J, CHEN G L. Effects of Nb and Al on the microstructures and mechanical properties of high Nb containing TiAl base alloys [J]. Intermetallics, 2002, 10: 653−659.

[7] OUYANG Si-hui, LIU Bin, LIU Yong, ZAN Xiang, LIANG Xiao-peng, LI Zheng. Dynamic tensile behavior of PM Ti−47Al−2Nb−2Cr−0.2W intermetallics at elevated temperatures [J]. Transactions of Nonferrous Metals Society of China, 2019, 29: 1252−1262.

[8] QU H P, LI P, ZHANG S Q, LI A, WANG H M. The effect of heat treatment on the microstructure and mechanical property of laser melting deposition *γ*-TiAl intermetallic alloys [J]. Materials & Design, 2010, 31: 2201−2210.

[9] KAWABATA T, FUKAI H, IZUMI O. Effect of ternary additions on mechanical properties of TiAl [J]. Acta Materialia, 1998, 46: 2185−2194.

[10] XIANG Liu-yi, WANG Fen, ZHU Jian-feng, WANG Xiao-feng. Mechanical properties and microstructure of Al_2O_3/TiAl in situ composites doped with Cr_2O_3 [J]. Materials Science and Engineering A, 2011, 528: 3337−3341.

[11] SUN F S, CAO C X, KIM S E, LEE Y T, YAN M G. Alloying mechanism of beta stabilizers in a TiAl alloy [J]. Metallurgical and Materials Transactions A, 2001, 32: 1573−1589.

[12] LIU Q, NASH P. The effect of Ruthenium addition on the microstructure and mechanical properties of TiAl alloys [J]. Intermetallics, 2011, 19: 1282−1290.

[13] LIU Z G, CHAI L H, CHEN Y Y. Effect of cooling rate and Y element on the microstructure of rapidly solidified TiAl alloys [J]. Journal of Alloys and Compounds, 2010, 504(S): s491−s495.

[14] KLEIN T, SCHACHERMAYER M, MENDEZ-MARTIN F, SCHOBERL T, RASHKOVA B, CLEMENS H, MAYER S. Carbon distribution in multi-phase *γ*-TiAl based alloys and

its influence on mechanical properties and phase formation [J]. Acta Materialia, 2015, 94: 205−213.
[15] NISHIKIORI S, MATSUDA M, NAKAGAWA Y G. Microstructural effects on tensile properties of cast TiAl−Fe−V−B alloy [J]. Materials Science and Engineering A, 1997, 239−240: 592−599.
[16] QIU Cong-zhang, LIU Yong, HUANG Lan, ZHANG Wei, LIU Bin. Effect of Fe and Mo additions on microstructure and mechanical of TiAl based intermetallics [J]. Transactions of Nonferrous Metals Society of China, 2012, 22: 521−527.
[17] QIU Cong-zhang, LIU Yong, ZHANG Wei, LIU Bin, LIANG Xiao-peng. Development of Nb-free TiAl-based intermetallics with a low-temperature superplasticity [J]. Intermetallics, 2012, 27: 46−51.
[18] NAZAROVA T I, IMAYEV V M, IMAYEV R M FECHTH J. Study of microstructure and mechanical properties of Ti−45Al−(Fe,Nb) [J]. Intermetallics, 2017, 82: 26−31.
[19] NAZAROVA T I, IMAYEVV M, IMAYEV R M. Microstructure and mechanical properties of the Ti−45Al−5Fe intermetallic alloy [J]. Russian Physics Journal, 2015, 58: 797−802.
[20] MCCUSKER L B, von DREELE R B, COX D E, LOUER D, SCARDI P. Rietveld refinement guidelines [J]. Journal of Applied Crystallography, 1999, 32: 36−50.
[21] YANG Hui-min, SU Yan-qing, LUO Liang-shun, CHEN Hui, GUO Jing-Jie, FU Heng-zhi. Influences of Fe and B on the columnar structure of Ti46Al alloys [J]. Rare Metal Materials and Engineering, 2012, 41: 570−574.
[22] BELOV N A, AKOPYAN T K,BELOV V D,GERSHMAN J S, GORSHENKOV M V. The effect of Cr and Zr on the structure and phase composition of TNM gamma titanium aluminide alloy [J]. Intermetallics, 2017, 84: 121−129.
[23] XU Wen-chen, HUANG Kai, WU Shi-feng, ZONG Ying-ying, SHAN De-bin. Influence of Mo content on microstructure and mechanical properties of β-containing TiAl alloy [J]. Transactions of Nonferrous Metals Society of China, 2017, 27: 820−828.
[24] SHU Shi-li, QIU Feng, TONG Cun-zhu, SHAN Xiao-lan, JIANG Qi-chuan. Effects of Fe, Co and Ni elements on the ductility of TiAl alloy [J]. Journal of Alloys and Compounds, 2014, 617: 302−305.
[25] HAO Y L, CAO R, CUI Y Y, LI D. The effect of Ti−Al ratio on the site occupancies of alloying elements in γ-TiAl [J]. Intermetallics, 2000, 8: 633−636.
[26] DING X F, LIN J P, QI H, ZHANG L Q, SONG X P, CHEN G L. Microstructure evolution of directionally solidified Ti−45Al−8.5Nb−(W, B, Y) alloys [J]. Journal of Alloys & Compounds, 2011, 509: 4041−4046.
[27] CHEN G L, XU X J, TENG Z K, WANG Y L, LIN J P. Microsegregation in high Nb containing TiAl alloy ingots beyond laboratory scale [J]. Intermetallics, 2007, 15: 625−631.
[28] DING X F, LIN J P, ZHANG L Q, WANG H L, HAO G J, CHEN G L. Microstructure development during directional solidification of Ti−45Al−8Nb alloy [J]. Journal of Alloys and Compounds, 2010, 506: 110−119.
[29] CHUBB S R, PAPACONSTANTOPOULOS D A, KLEIN B M. First-principles study of L10 Ti−Al and V−Al alloys [J]. Physical Review B, 1988, 38: 12120−12124.
[30] DLOUHÝ I, CHLUP Z, HADRABA H. Fracture behaviour of TiAl intermetalics [M]. Heidelberg: Springer, 2009: 265−274.
[31] DUAN Qiu-qi, LUAN Qing-dong, LIU Jing, PENG Liang-ning. Microstructure and mechanical properties of directionally solidified high-Nb containing Ti−Al alloys [J]. Materials & Design, 2010, 31: 3499−3503.
[32] ALLINGER N L, ZHOU X, BERGSMA J. Molecular mechanics parameters [J]. Journal of Molecular Structure, 1994, 1: 69−83.
[33] BATSANOVS S. Atomic radii of elements [J]. Russian Journal of Inorganic Chemistry, 1991, 36: 3015−3037.
[34] CHAN K S. Toughening mechanisms in titanium aluminides [J]. Metallurgical and Materials Transactions A, 1993, 24: 569−582.
[35] XU X J, LIN J P, TENG Z K, WANG Y L, CHEN G L. On the microsegregation of Ti−45Al−(8−9)Nb−(W,B,Y) alloy [J]. Materials Letters, 2007, 61: 369−373.
[36] XU Zheng-feng, XU Xiang-jun, LIN Jun-pin, ZHANG Yong, WANG Yan-li, LIN Zhi, CHEN Guo-liamg. Homogenization treatment of high Nb containing TiAl alloys with as-cast and as-forged microstructures [J]. Rare Metals, 2015, 27: 181−186.

添加 Fe 元素改善 TiAl−Nb 合金的显微组织和力学性能

杨 勇[1,2]，冯和平[3]，王 琪[1]，陈瑞润[1]，郭景杰[1]，丁宏升[1]，苏彦庆[1]

1. 哈尔滨工业大学 材料科学与工程学院，哈尔滨 150001；2. 包头职业技术学院 材料工程系，包头 014030；
3. 内蒙古第一机械集团股份有限公司 第五分公司，包头 014032

摘 要：为了提高 TiAl−Nb 合金的力学性能并优化合金成分，熔炼制备不同含 Fe 量(0, 0.3, 0.5, 0.7, 0.9 和 1.1，摩尔分数，%)Ti46Al5Nb0.1B 合金试样，系统研究合金的宏观/显微组织及压缩力学性能。结果表明，Fe 元素能细化晶粒、加重枝晶间的铝偏析并在枝晶间形成富铁 *B*2 相。室温压缩实验结果表明，合金 Ti46Al5Nb0.3Fe0.1B 具有最高的极限压缩强度和断裂应变，分别为 1869.5 MPa 和 33.53%。晶粒细化及 Fe 元素的固溶强化能提高合金的压缩强度，γ 相晶胞四方度降低及晶粒细化能提高合金的断裂应变；然而，添加过量 Fe 元素导致的铝偏析会降低合金的压缩强度和断裂应变。

关键词：TiAl 合金；Fe；*B*2 相；显微组织；力学性能

(Edited by Wei-ping CHEN)